J. Appl. Comput. Mech., 6(4) (2020) 741-756
DOI: 10.22055/JACM.2018.26277.1316

ISSN: 2383-4536
jacm.scu.ac.ir

M&MoCS

Shahid Chamran University of Ahvaz

Journal of Applied and Computational Mechanics

Research Paper

Fluid Flow and Heat Transfer over Staggered '+' Shaped Obstacles

Younes Menni[1], **Ali J. Chamkha**[2], **Ahmed Azzi**[1,3]

[1] Unite of Research on Materials and Renewable Energies, Department of Physics, Faculty of Sciences, Abou Bekr Belkaid University BP 119-13000-Tlemcen, Algeria

[2] Faculty of Engineering, Kuwait College of Science and Technology, Doha, Kuwait

[3] Department of Mechanical Engineering, Faculty of Technology, Abou Bekr Belkaid University BP 230-13000-Tlemcen, Algeria

Received June 18 2018; Revised December 15 2018; Accepted for publication December 15 2018.
Corresponding author: Y. Menni (menniyounes.cfd@gmail.com)

Abstract. The inclusion of complex obstacles within solar channels is the aim of this article. Two obstacles of the form '+' interlaced within a two-dimensional and rectangular channel are the subject of our study. The fluid is Newtonian, turbulent, incompressible and has constant properties. The Reynolds number varies from 12,000 to 32,000 with a constant temperature along the upper surface of the channel. The thermal and dynamic analysis of the channel's internal structure has been carefully processed. Different fields of speed and heat, with various profiles of frictions and heat exchange coefficients, have been included in this research. Future work will involve more complex geometries and using nanofluids to assess the optimum conditions for heat transfer enhancements.

Keywords: Heat exchange, Friction, Fluid flow, Complex obstacle, Reynolds number, Nusselt number.

1. Introduction

Fluid flow and heat transfer in solar air channels received considerable interest during the last several decades. The first numerical work investigating the flow and heat transfer characteristics in ducts with the periodically fully developed flow concept was presented by Patankar et al. [1]. Kelkar and Patankar [2] numerically computed the fluid flow and heat transfer behaviors of air in a parallel plate channel with staggered fins. These authors concluded that the flow is characterized by strong deformations and large recirculation cells. In general, convective Nusselt number and pressure drop increase with the flow Reynolds number. The numerical computation of conjugate heat transfer characteristics for a constant property fluid flowing laminarly through a parallel plate channel with staggered, transverse ribs and a constant heat flux along both walls, based on the periodically fully developed flow conditions of Patankar et al. [1], was conducted by Webb and Ramadhyani [3]. Their results showed the same behavior as Kelkar and Patankar [2]. Lopez et al. [4] investigated three-dimensional effects for this same geometry and obtained similar results as those taken at the center of the channel. A calculation method was developed by De Zilwa et al. [5] and used to represent flows downstream of plane-symmetric expansions with dimensions and velocities encompassing laminar and turbulent flows. The turbulent flow simulations using k-ε turbulence model showed to be reliable when compared to experimental results, except in regions close to the wall and within the recirculation regions, underestimating the reattachment location. Hong and Hsieh [6] investigated the combined effects of rib alignment and channel aspect ratio on the distributions of the local heat transfer coefficient and on the friction factors for developing and fully developed flow in short square and rectangular channels with a pair of opposite rib-roughened walls. In that study, the channel aspect ratios were 0.5 and 1

Published online: September 28 2019

and the rib alignment configurations were arranged as staggered and in-line types, respectively. Semi-empirical heat transfer and friction correlations were developed, and the results were compared with those of previous investigations for similarly configured channels, which were roughened by regularly spaced transverse ribs. Two general turbulence models, the standard k-ε model, and the Reynolds stress model were used by Luo et al. [7] to predict the forced convection of a fully developed turbulent flow through an assembly of two horizontally oriented parallel plates with periodic transverse ribs. The investigations revealed that in the simulation of the turbulent forced convection in this two-dimensional channel with a ribbed surface, the standard k-ε model had superiority over the Reynolds stress model. They found that the anticlockwise vortex was observed in the downstream region of a rib by using either of two models while the length and relative strength of the vortex predicted by these two models were significantly different. An experimental study was conducted by Molki and Mostoufizadeh [8] to investigate heat transfer and pressure losses in a rectangular duct with repeated-baffle blockages. In that study, the baffles were arranged in a staggered fashion with fixed axial spacing. The transfer coefficients were evaluated in the periodic fully developed and entrance regions of the duct. They concluded that the entrance length of the duct is substantially reduced by the baffles. Cheng and Huang [9] again presented laminar fluid flow and forced convection heat transfer in the entrance region of a horizontal channel with one or two pairs of transverse baffles placed on the walls. Parameters of the numerical work were the Reynolds number and the baffle geometric arrangement. In addition to the velocity, temperature, and vorticity distributions, local heat transfer performance was evaluated, and a comparison of the results between the channels with and without transverse fins was also made. Another numerical investigation was carried out by Guo and Anand [10] to calculate laminar heat transfer and pressure drop in a three-dimensional channel with a single baffle in the entrance region. The parametric runs focused on the effects of Reynolds number, Prandtl number, thermal conductivity ratio, and baffle height on the laminar forced convection measurements. Their results showed that the separation length upstream of the baffle and the recirculation length downstream of the baffle increased with an increase in the flow Reynolds number and baffle height. In general, the spanwise averaged Nusselt number increased with an increase in the thermal conductivity of the wall. Also, Mousavi and Hooman [11] carried out a numerical investigation of laminar flow filed and convective heat transfer characteristics in the entrance region of a two-dimensional horizontal channel with isothermal walls and with staggered baffles. In that study, different flow Reynolds and Prandtl numbers and different baffle heights were examined. The results were reported for the thermal entrance region with sixteen baffles. The results demonstrated that the increase of flow Reynolds number yields to the removal of a higher quantity of energy from baffle faces. The results also demonstrated that increasing the baffle height makes the flow deviate and accelerate in the vicinity of faces and cause an increase in the rate of convective heat transfer from baffles. These authors also reported that the Prandtl number affect the precise location of the periodically fully developed region similar to the case of the smooth channel. Experimental investigations on flow friction and convective heat transfer enhancement in shell-and-tube heat exchangers with baffle plates orthogonal to the flow direction have been carried out extensively. Founti and Whitelaw [12] employed the Laser-Doppler anemometry technique to deduce the velocity field in an axisymmetric shell-and-tube heat exchanger with transverse baffles on the shell-side surface. The similar distributions of the mean velocity and turbulence intensity were found after two sets of baffles from the channel entrance. Flow visualization, manometer, and laser-Doppler anemometry have been applied by Berner et al. [13, 14] to approximately two-dimensional flow around segmental baffles with Reynolds numbers ranging from 600 to 10.500 to simulate important aspects relating to shell-side flow in shell-and-tube heat exchangers. In those studies, the main features of the flow, development lengths, pressure loss coefficients, and mean velocity distributions were presented. Velocity and turbulence measurement using hot-wire technique in the turbulent flow over prisms with several aspects rations were performed by Antoniou and Bergeles [15]. By increasing the aspect ratio L/H, the flow reattaches on the prism surface and downstream, while recirculation lengths and turbulence scales are reduced. Heat transfer measurements and predictions were reported by Acharya et al. [16] for a turbulent, separated duct flow past a wall-mounted two-dimensional rib. The computational results included predictions using the standard k-ε model, the algebraic-stress (A-S) functionalized k-ε model, and the nonlinear k-ε model. The experiments included Laser-Doppler flow measurements, temperature measurements, and local Nusselt number results. As a result of their study, they reported that the AS functionalized model using only the high Reynolds number formulation and curvature correlations in Cartesian coordinates improved the temperature predictions substantially, with the predicted flow temperatures agreeing quite well with the measured temperatures. Möller et al. [17] presented the experimental study of the wall pressure distribution and the behavior of pressure and velocity fluctuations in the turbulent flow of air through a simulated tube bank with the square arrangement, after passing a baffle plate. The experimental results of velocity fluctuations and wall pressure fluctuations were obtained through hot wires and a pressure transducer. In general, results of wall pressure and wall pressure fluctuations showed higher values than in pure cross-flow as demonstrated by Endres [18], and Endres and Möller [19]. By means of hot wire experiment and numerical simulations, Demartini [20], and Demartini et al. [21] reported the analysis of the pressure and velocity fields in the same test section as described in Möller et al. [17], and Endres and Möller [19], but the tube bank was removed, to allow the study of the flow on the baffle plates. Low and high-pressure regions were associated with recirculation regions. The most intense was that occurring behind the second baffle plate, responsible for the high flow velocities observed at the outlet of the test section, creating a negative velocity profile which introduced mass inside the test section through the outlet. Another experimental investigation was carried out by Habib et al. [22] to evaluate the characteristics of the turbulent flow and heat transfer inside the periodic cell formed between segmented baffles staggered in a rectangular channel. The experiments focused on the influence of Reynolds number and baffle height on the local and average heat transfer

coefficients, and flow friction measurements. Their results demonstrated that for a constant value of the Reynolds number, the pressure loss increased as the baffle height did. Also, the local and average heat transfer parameters increased with increasing Reynolds number and baffle height. Effect of baffle spacing on the hydrodynamic and thermal parameters in simulating models of shell-and-tube heat exchangers was experimentally reported by Li and Kottke [23]. They found that for a given flow rate, increasing the distance between the baffles increased the heat exchange coefficient and the pressure drop. Aiming to enhance the heat transfer characteristics of backward-facing step flow in a channel, Tsay et al. [24] proposed a method to install a baffle onto the channel wall. The effects of the dimensionless baffle height, baffle thickness, and distance between the backward-facing step, and baffle on the hydrodynamic and thermal behaviors was numerically studied in detail for a range of Reynolds number varying from 100 to 500. These authors found that insertion of a baffle into the flow increases the average Nusselt number by 190%. They also observed that the flow conditions and heat transfer characteristics are a strong function in the baffle position. Other authors studied in detail the effect of baffle shape geometries and their orientations on the heat transfer enhancement in the heat exchanger channels. Promvonge and Thianpong [25] conducted the effect of various rib shapes (i.e., wedge, triangular and rectangular-shaped) on thermal behaviors in a channel, and reported that the staggered triangular rib performs the best. Sripattanapipat and Promvonge [26] numerically examined the laminar periodic flow and thermal comportment in a two-dimensional channel fitted with staggered diamond-shaped baffles and found that the diamond baffles with half apex angle of 5°-10° perform slightly better than the flat baffles for all Reynolds number used. Effects of 45° staggered V-shaped baffles on periodic laminar flow and heat transfer characteristics in a channel, were reported by Promvonge and Kwankaomeng [27]. The results showed that the optimum thermal enhancement factor is around 2.6 at a baffle height of 0.15 times of the channel height for V-baffle pointing upstream while is about 2.75 at a baffle height of 0.2 times for the V-baffle pointing downstream. The influence of baffle turbulators on heat transfer augmentation in a rectangular channel was investigated experimentally and numerically by Sriromreun et al. [28]. In the experiment, the baffles were placed in a zigzag shape (Z-shaped baffle) aligned in series on the isothermal-fluxed top wall, similar to the absorber plate of a solar air heater channel. Thermal and hydrodynamic parameters were examined numerically and experimentally by Lei et al. [29] for a flow passing through a channel with only one helical-shaped baffle. A comparative study, between three different channels, was conducted by those authors. In the first case, a channel without any baffles examined. In the second case, the same channel with only one helical baffle considered. In the third case, the same channel with two helical baffles investigated. Another study reported by Gupta et al. [30]. These authors used a helical-shaped baffle in a mineral (Carbosep) membrane provided an increase of more than 50% in permeate flux compared with that obtained without a baffle at the same hydraulic dissipated power. Benzenine et al. [31] simulated the turbulent airflow and conjugate heat transfer in a rectangular duct provided with waved fins, which arranged on the bottom and top channel walls in a periodically staggered way. Since that work emphasized on baffles that directly block the flow, the pressure penalties are higher than the heat transfer improvements. However, it is possible to obtain enhanced heat transfer with comparably less frictional heat loss by inserting inclined baffles, in the flow path. Inclined baffles may be considered as a combination of baffles and channel inserts. These baffles are big enough to disturb the core flow, but like baffles, they mounted on or near the heat transfer surface. In this context, Nasiruddin and Kamran Siddiqui [32] numerically investigated three different orientations of baffles; the first case is a vertical baffle, the second inclined towards the downstream side, and the third inclined towards the upstream side. The results showed that for the vertical baffle, an increase in the baffle height causes a substantial increase in the Nusselt number but the pressure loss is also very significant. For the inclined baffles, the results showed that the Nusselt number enhancement is almost independent of the baffle inclination angle, with the maximum and average Nusselt number 120% and 70% higher than that for the case of no baffle, respectively. Moreover, inclined perforated baffles contain circular holes, which facilitate jet impingement toward the heat transfer surface. Hence by utilizing inclined perforated baffles, the three major heat transfer augmentation techniques can be combined for effective cooling. Dutta [33], Dutta and Dutta [34], and Dutta et al. [35] reported the enhancement of heat transfer with inclined solid and perforated baffles. In those studies, the effects of baffle size, position, and orientation with different aspect ratio channels and different porosity baffle studied for internal cooling heat transfer augmentation.

In this current simulation, we propose to make a computational fluid dynamic analysis of fluid flow and thermal transfer characteristics over complex obstacles in solar air channels. Two obstacles of the form '+' interlaced within a two-dimensional and rectangular channel are the subject of our study. The fluid is Newtonian, turbulent, incompressible, and has constant properties. The number of Reynolds varies from 12,000 to 32,000 with a constant temperature along the upper surface of the channel. The thermal and dynamic analysis of the channel's internal structure has been carefully processing. Different fields of speed and heat, with various profiles of frictions and heat exchange coefficients, have been included in this research.

2. Physical Model

The current main objective at employing the '+' obstacles is to force recirculations having a significant impact on the turbulence structure leading to upper thermal transfer improvement in the solar air channel. A schematic representation of the physical model is shown in Fig.1. The numerical domain is a modification of the test section employed in Demartini et al. [21], where the airflow was deflected by a simple baffle, being a 0.554m long (L) horizontal two-dimensional channel, with a height (H) of 0.146m. Two '+' obstacles are introduced into the channel field to force

recirculation zones, to enhance the mixture and thus, the thermal transfer. The first '+' obstacle is attached to the hot wall of the channel at a distance of L_{in} = 0.218m from the upstream end of the channel. A second '+' obstacle is placed on the opposite channel wall, 0.142m (or *Pi*) after the first '+' obstacle, in the other extremity of the channel, 0.174m (or L_{out}) before channel outlet. The distance between the top edge of the '+' obstacles and the channel wall is kept constant at h = 0.08m. The Prandtl number (Pr) is taken equal to 0.71. To simplify the problem, some assumptions are considered:

- Steady two-dimensional fluid flow and heat transfer.
- The flow is turbulent and incompressible.
- The thermo-physical properties of the fluid assumed to be constant.
- The upper channel wall subjected to a constant wall temperature.
- Uniform velocity applied at the inlet of the channel and air is selected as working fluid.
- Body forces, viscous dissipation, and radiation heat transfer ignored.

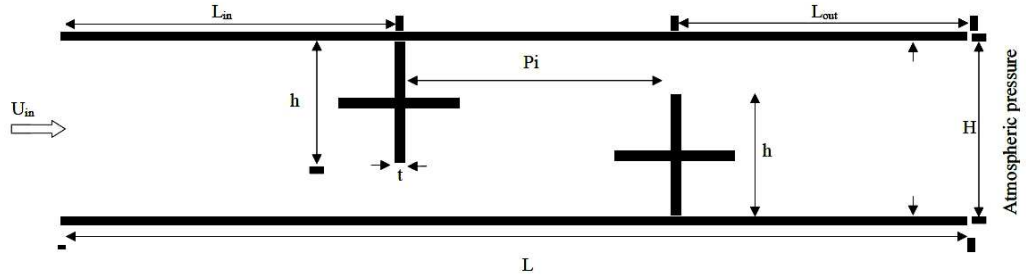

Fig. 1. Complex baffled channel.

Based on the above assumptions, the continuity, momentum, and energy equations used to simulate the fluid flow and thermal transfer in the given solar air channel given as:

$$\nabla.\vec{V} = 0 \tag{1}$$

$$\rho\left(\vec{V}.\nabla\vec{V}\right) = -\nabla P + \mu_f \nabla^2 \vec{V} \tag{2}$$

$$\rho.C_p\left(\vec{V}.\nabla T\right) = \lambda_f \nabla^2 T \tag{3}$$

where $\vec{V}$ represents the velocity vector, ρ is the fluid density, P is the pressure, μ_f is the dynamic viscosity of fluid, C_p is the specific heat at constant pressure, and λ_f is the fluid thermal conductivity. The Shear-Stress Transport (SST) k-ω model [36] is defined by two transport equation, one for the turbulent kinetic energy, k and the other for the specific dissipation rate ω, as given below:

$$\frac{\partial}{\partial x_i}(\rho k u_i) = \frac{\partial}{\partial x_j}\left(\Gamma_k \frac{\partial k}{\partial x_j}\right) + G_k - Y_k + S_k \tag{4}$$

$$\frac{\partial}{\partial x_i}(\rho \omega u_i) = \frac{\partial}{\partial x_j}\left(\Gamma_\omega \frac{\partial \omega}{\partial x_j}\right) + G_\omega - Y_\omega + D_\omega + S_\omega \tag{5}$$

In these equations, G_k represents the generation of turbulence kinetic energy due to mean velocity gradients. G_ω represents the generation of ω. Γ_k and Γ_ω are the effective diffusivity of k and ω, respectively. Y_k and Y_ω represent the dissipation of k and ω due to turbulence. D_ω is the cross-diffusion term. S_k and S_ω are user-defined source terms.

A uniform one-dimensional velocity profile (U_{in}) was employed as the aeraulic boundary condition at the intake of the computational domain. The temperature (T_{in}) of the working fluid was set equal to 300K at the inlet of the channel. The thermal boundary condition consisted of the constant temperature (T_w) of 375K which was applied to the upper wall of the computational domain. The bottom surface of the computational domain was taken as adiabatic. Moreover, it was decided to impose the no-slip and impermeability boundary conditions at all the solid walls. Note that the atmospheric pressure (P_{atm}) is prescribed at the channel outlet.

3. Numerical Model

The governing equations, based on Shear-Stress Transport k-ω model [36], were integrated and discretized according to the approach of finite volume method [37], to convert the governing equations to algebraic equations that can be solved numerically. Given the characteristics of the flow, the Quick-numerical scheme applied to the interpolations, while a scheme of Second-Order used for the pressure terms. The Reynolds number defined as:

$$\mathrm{Re} = \frac{\rho \overline{U} D_h}{\mu} \tag{6}$$

The skin friction coefficient, *Cf is* given by:

$$Cf = \frac{\tau_w}{\frac{1}{2}\rho \overline{U}^2} \tag{7}$$

The friction factor, f is computed by pressure drop, ΔP across the length of the channel, L having the aeraulic diameter, $D_h = 0.167$m as:

$$f = \frac{(\Delta P/L) D_h}{\frac{1}{2}\rho \overline{U}^2} \tag{8}$$

and the friction factor for a smooth channel is calculated from the correlation developed by Petukhov [38] as follows:

$$f_0 = \left(0.79 \ln \mathrm{Re} - 1.64\right)^{-2} \quad \text{for} \quad 3{,}000 \le Re \le 5\times 10^6 \tag{9}$$

The local Nusselt number, Nu_x is evaluated as follows:

$$Nu_x = \frac{h_x D_h}{\lambda_f} \tag{10}$$

The average Nusselt number, Nu can be obtained by:

$$Nu = \frac{1}{L}\int Nu_x \partial x \tag{11}$$

The average Nusselt number of a smooth channel as a reference for the study is calculated using the correlation of Dittus and Boelter [39], which shows a consistent agreement with low Reynolds number and is given by:

$$Nu_0 = 0.023\,\mathrm{Re}^{0.8}\,\mathrm{Pr}^{0.4} \quad \text{for} \quad Re \ge 10{,}000, \text{ heating} \tag{12}$$

where $\overline{U}$ is the average axial velocity of the section, τ_w is the wall shear stress, and h_x represents the local convective heat transfer coefficient.

To verify the numerical results of this simulation, we compared the pressure coefficients and the axial velocity values of this analysis with those given by the numerical and experimental study of Demartini et al [21] in the two different axial stations x = 0.233 m and x = 0.525 m, as shown in Fig. 2 (a) and (b), respectively.

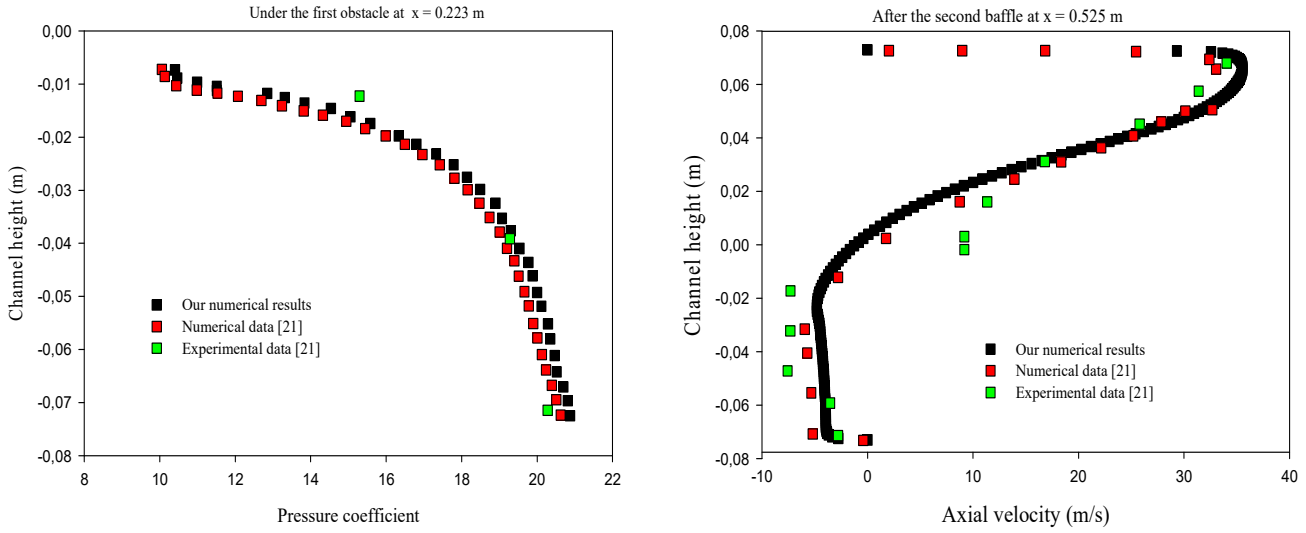

(a) (b)

Fig. 2. Comparison of (a) pressure coefficient and (b) axial velocity with the literature [21].

There is a quantitative and qualitative consensus between numerical and experimental data. This confirms the validity of the model used during this study.

4. Results and Discussion

Figure 3 shows the dynamic structure of the air inside the solar channel. The air enters by the constant axial velocity with regular and parallel lines. The introduction of obstacles of '+' form gives a turbulent and complex structure to the air current. The airflow path divided into two important paths; the first is the main from the input to the outlet with super speed, while the second is formed from a combination of secondary streams at a weak speed and for recycling areas. Each obstacle within the channel produces four recycling zones; two on the front and two on the back. These areas are characterized by the low speed with negative values due to current movement in the opposite direction and are small in size and weak in intensity. While the addition of the second obstacle adds a fifth large-scale, low-velocity and strong-intensity recycling zone, located between the two obstacles, precisely enclosed between the mainstream and the right side of the first obstacle. There is also a recycling area behind the second obstacle where it extends to the exit and features a large size, at a weak speed with an intensity neglected. The recycling areas are becoming more intense by increasing the number of Reynolds.

Figure 3 also allows the determination of the mean velocity values of the air current in different areas of the channel, whether from recycling areas or within the mainstream. The presence of the first obstacle causes a change in the direction of the current. The main air current shifts from the top of the channel to the lower side, passing under the upper side of the first obstacle until it collides with the second obstacle and then moves towards the top of the channel, passing over the top of the same obstacle until reaching the channel outlet with super speed, while the velocity value is very low next to the obstacles, especially on the left and right upper sides due to the recycling areas. There is a linear correlation between the increase in the number of Reynolds and the rise in velocity values.

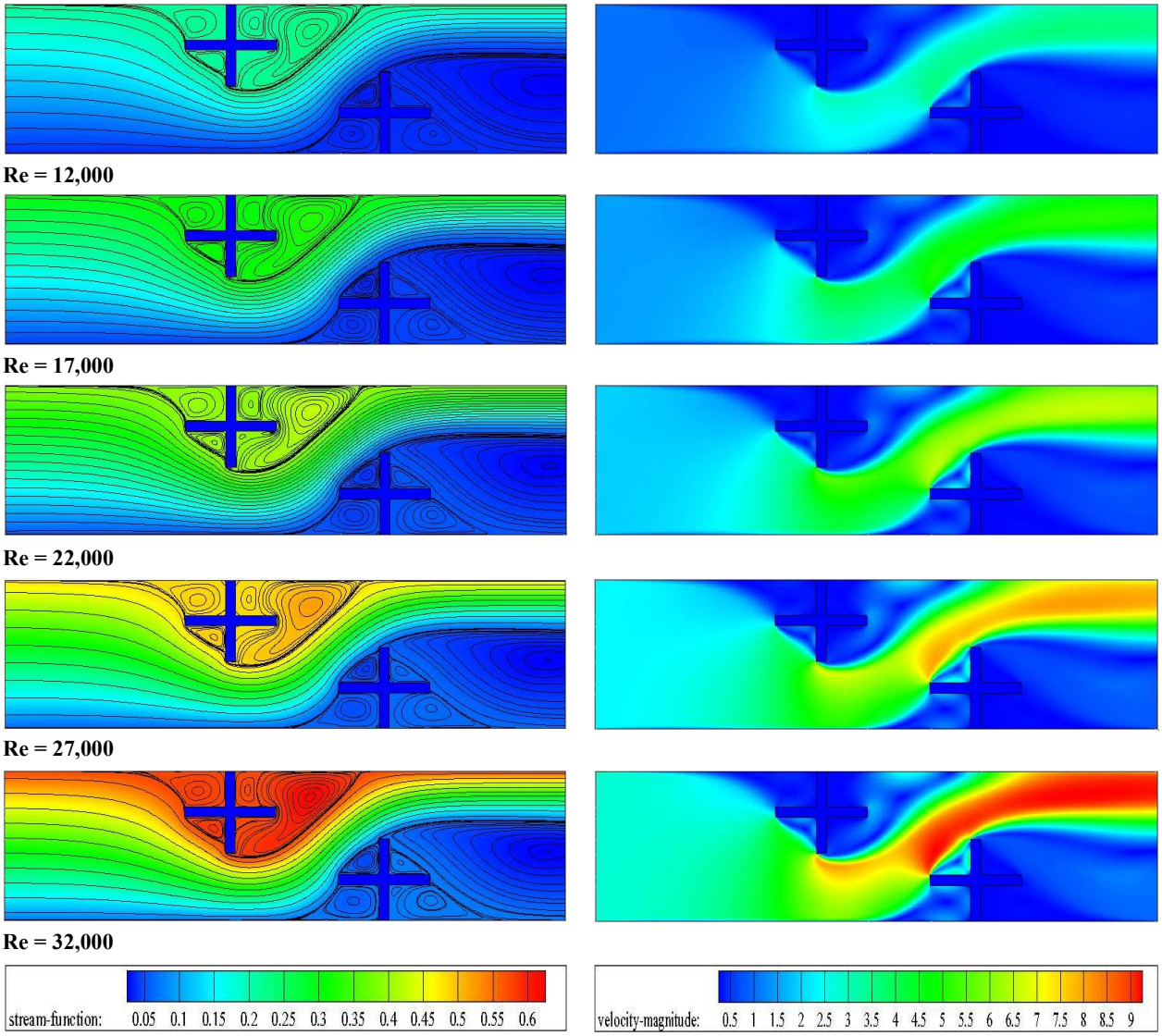

Fig. 3. Contours of fields of stream function and mean velocity as a function of Reynolds number.

The turbulent viscosity values in the channel inlet, and on the left and right sides of the first and second obstacles reduced respectively, Fig. 4. While the turbulent viscosity values in most points of the main airway are high because the flow direction changes rapidly due to the presence of the obstacles. The turbulent viscosity increased by increasing the number of Reynolds, especially near the left side of the second obstacle, as well as near the hot top surface of the channel above the same obstacle.

The high temperature of the air current near the hot surface of the channel especially at the level of the first obstacle in the recycling areas is evidence of good thermal exchange in this region of the channel. Positioning the first obstacle on the hot top surface of the channel allows contact between the hot walls of the obstacle and the air molecules and thus an important thermal exchange. While the presence of the second obstacle allows the deflection of the air current from the bottom of the channel near the thermally insulated bottom surface towards the hot end and thus collision and friction, then a good heat exchange with important thermal energy gained by the particles of air. The increase in the number of Reynolds increases the flow velocity and decreases the temperature of the air molecules, Fig. 4.

In order to better analyze the evolution of the air velocity in each region of the channel that is upstream, downstream and between the obstacles. We plotted dependence of axial velocity for these selected positions: x = 0159 m, x = 0.189 m, x = 0.255 m, x = 0.285 m, x = 0.315 m, x = 0,345 m, x = 0.465 m and x = 0.525 m, marked in Figs. 5 and 6.

Fig. 6 (a) represents the axial velocity profiles in the different transverse positions x = 0.159 m and x = 0.189 m of the channel entrance. These positions are located near the front of the first obstacle with distances of 0.059 m and 0.029 m, respectively. The speed values in the upper part of the channel are lowered, while in the lower part it rises through the first obstacle. Near the latter, located at a distance of 0.218 m from the entrance of the channel, the velocity values next to the same obstacle decrease due to the formation of two recycling zones with negative values of speed on the upper and lower front sides of the same obstacle. Also, a large part of the current leaks downwards under the upper side of the same obstacle but very quickly because of the narrow duct of the channel in this area.

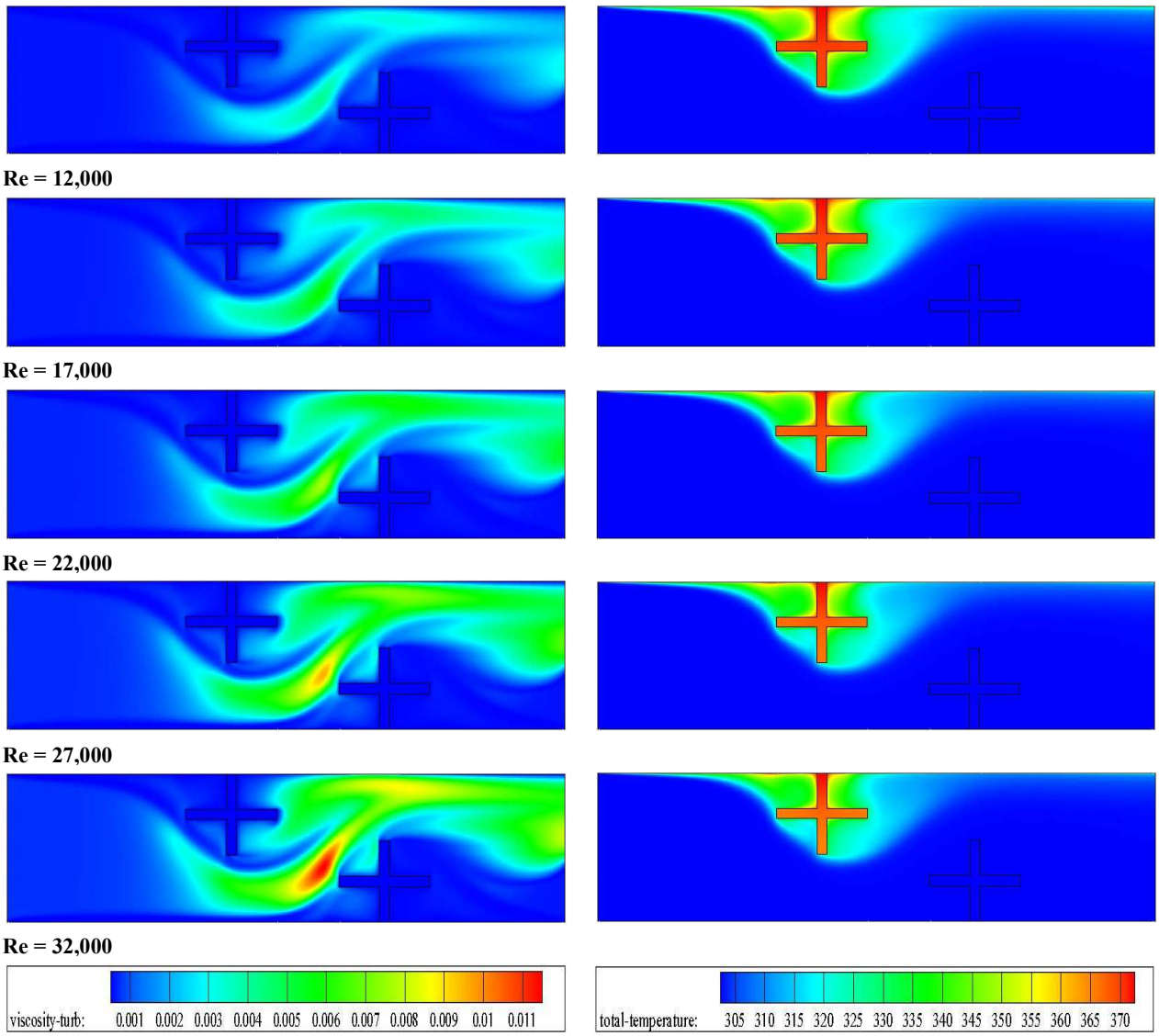

Fig. 4. Contours of fields of turbulent viscosity and temperature as a function of Reynolds number.

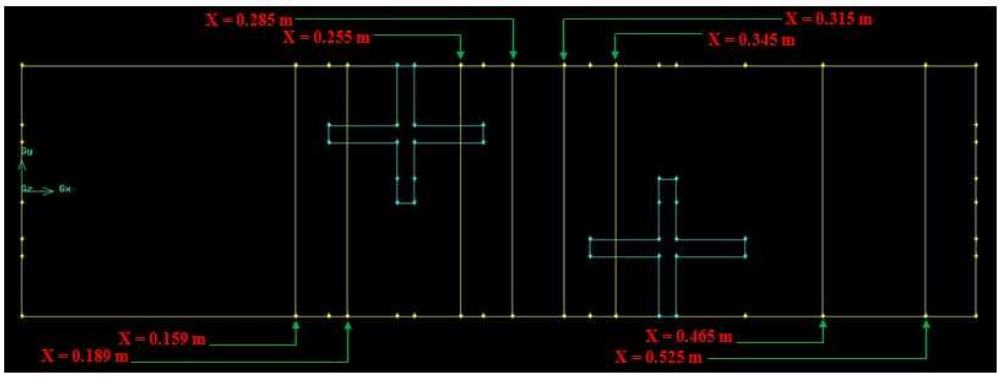

Fig. 5. Axial stations under investigation.

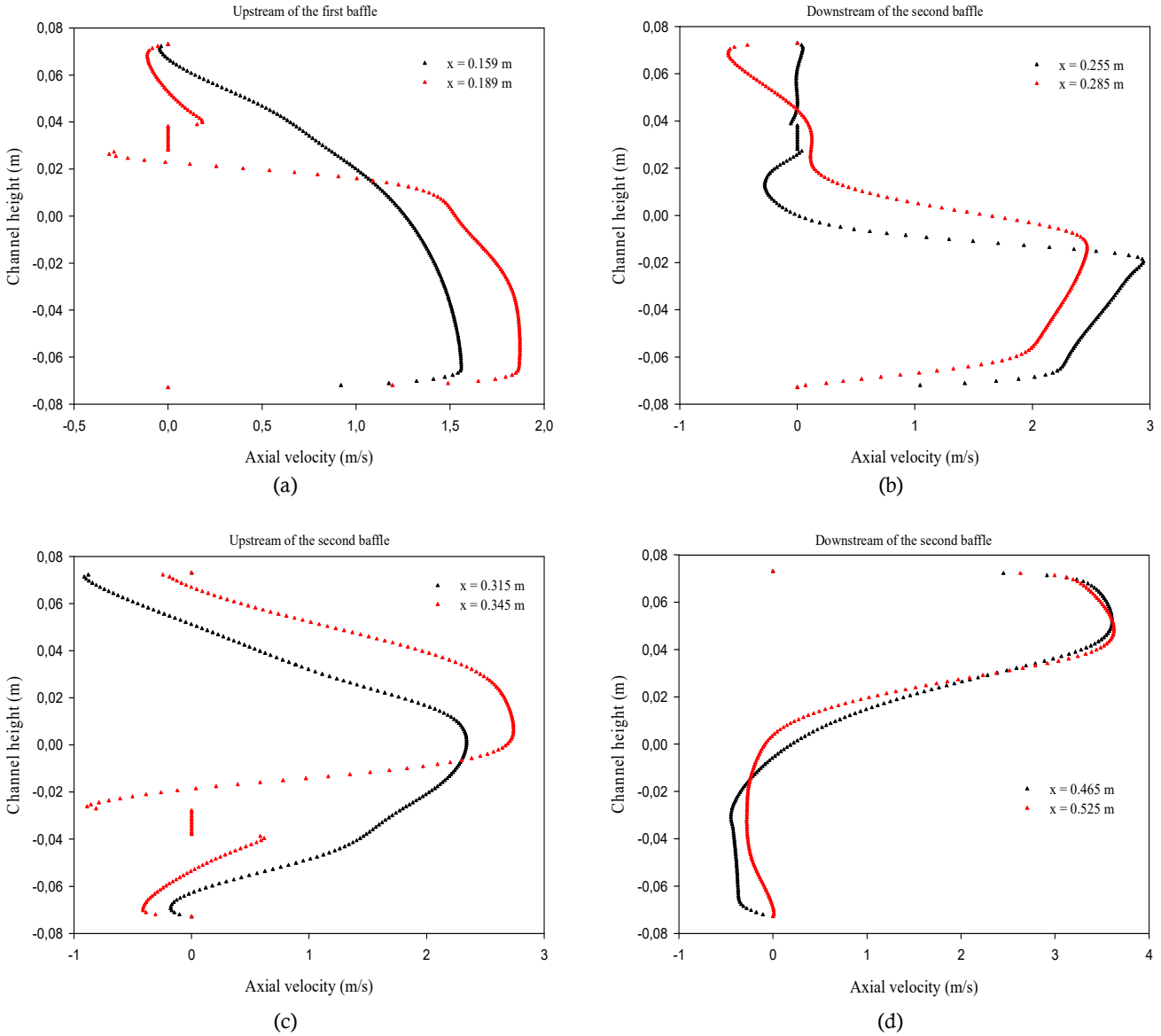

Fig. 6. Profiles of axial velocity at various axial stations in the channel for Re = 12,000.

Fig. 6 (b) shows the axial velocity profiles of the air particles at the back of the first obstacle in the axial positions x = 0.255 m and x = 0.285 m of the channel entrance, i.e., 0.027 and 0.057 after the first obstacle, respectively. The upper area of the speed profiles has weak and negative values. These values are indicative of the existence of three recycling zones in this area of the channel. Two recycling areas of small and very weak size near the right side of the first obstacle, while the third area of recycling is large and very strong, positioned between the obstacles to the right of the recycling areas in the upper and lower parts of the first obstacle, and to the left of the mainstream. While at the bottom of the studied positions, the velocity values are large but decreasing as close to the air current of the second obstacle.

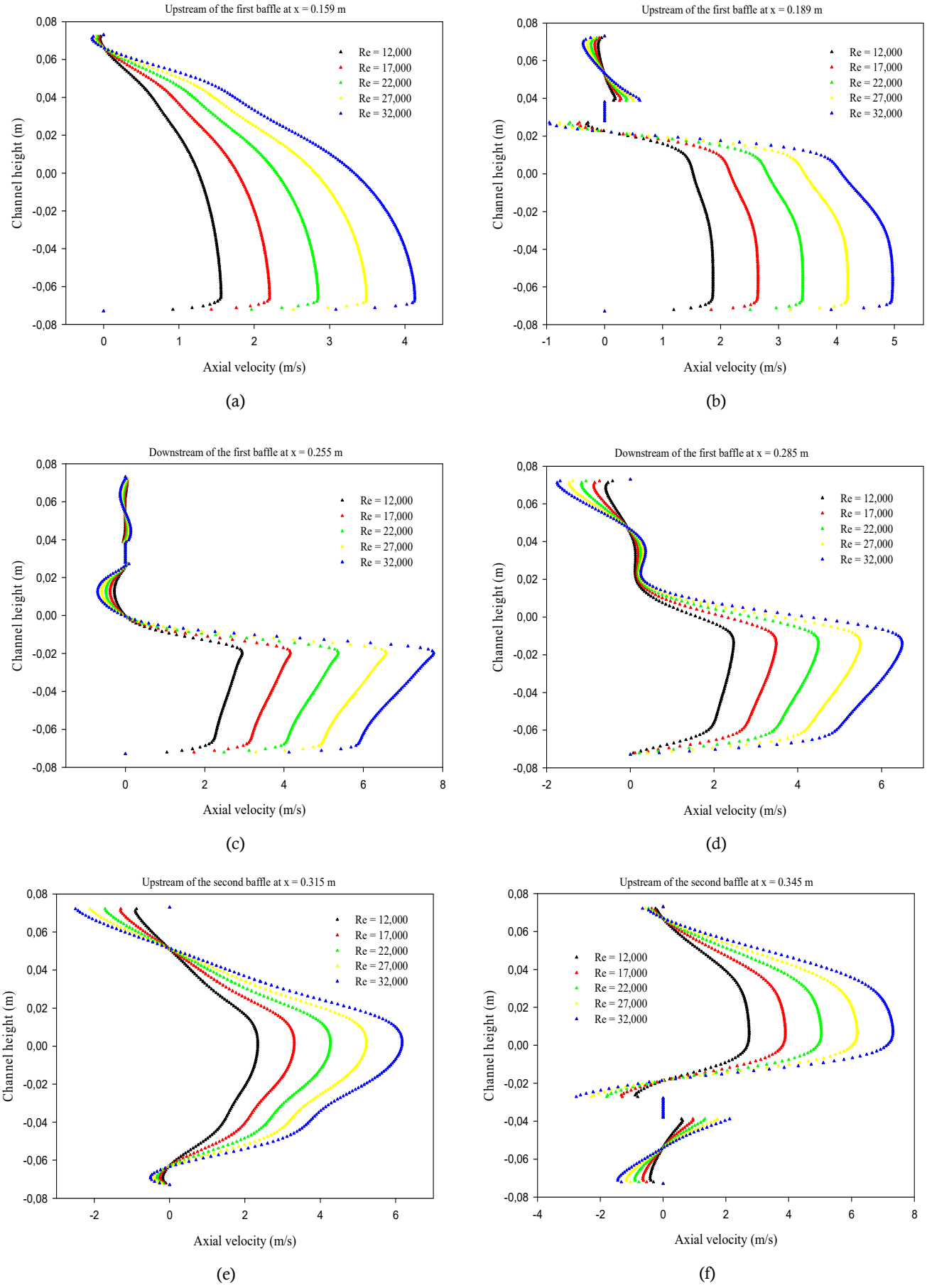

Fig. 7. Variation of axial velocity profiles with Reynolds number at various axial stations in the channel.

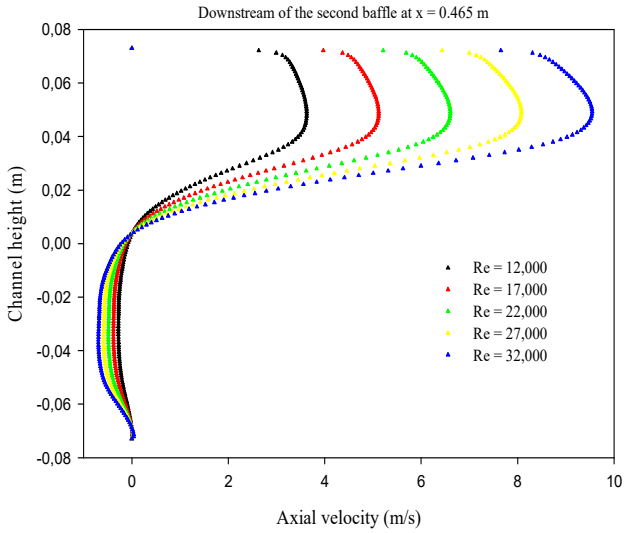

(g)

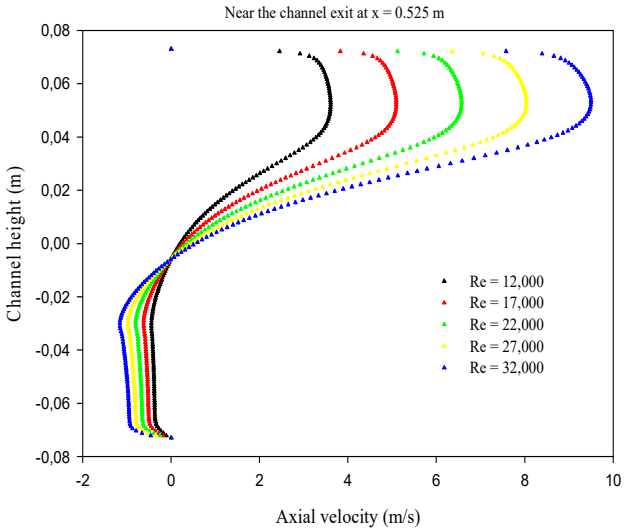

(h)

Fig. 7. Continued.

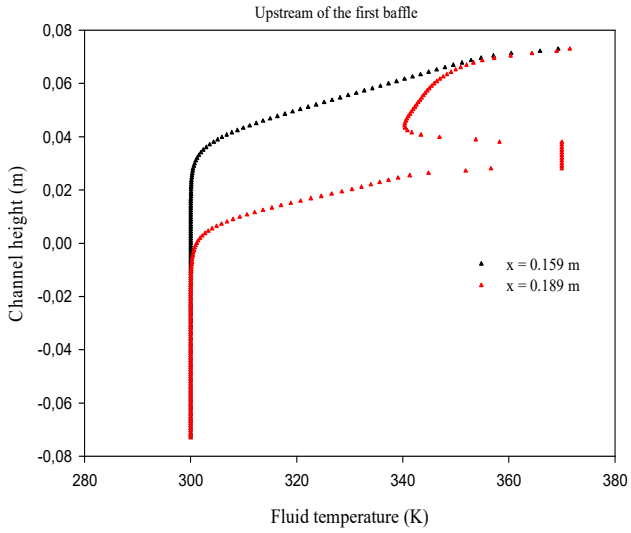

(a)

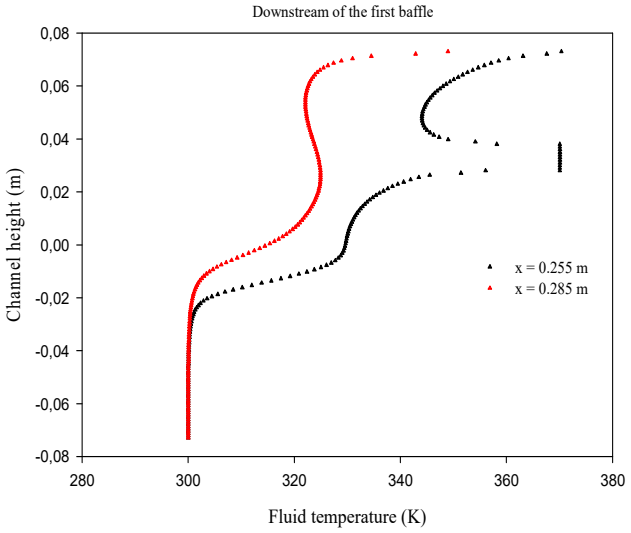

(b)

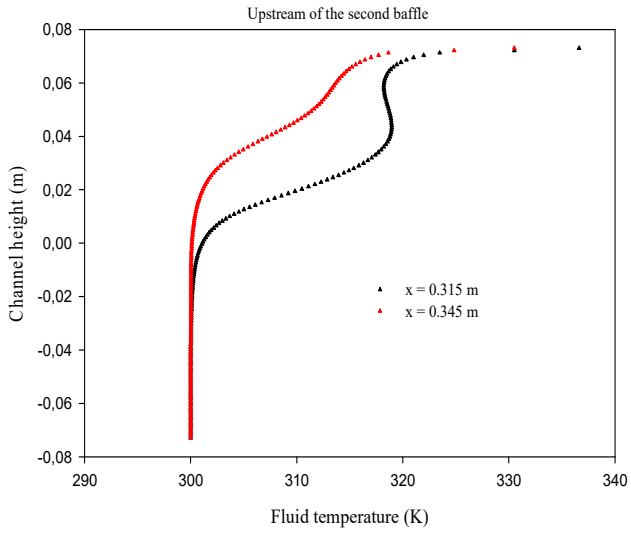

(c)

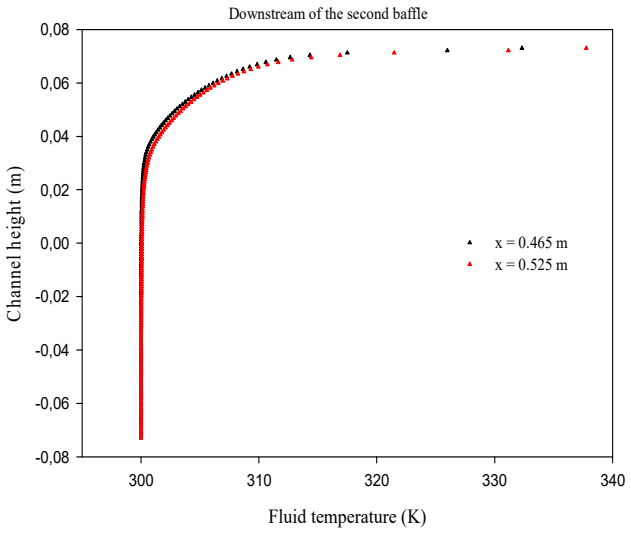

(d)

Fig. 8. Profiles of fluid temperature at various axial stations in the channel for Re = 12,000.

In the middle zone of the channel, between the upper and lower obstacles, at the axial stations x = 0.315 m and x = 0.345 m, the axial velocity profiles have negative values. Negative speeds in the two situations are studied guide along the recycling area in the central area of the canal near the surface of the hot top. While velocity values increase in the area confined between the upper surface of the channel and the second obstacle due to the presence of the latter. In the lower region of the front of the second obstacle, the velocity values decrease due to current flow in the opposite direction, because there are two recycling areas of small size and a weak intensity on the left side in the upper and lower parts of the same obstacle, Fig. 6 (c).

Next to the right side of the second obstacle in transverse position x = 0.465 m, and near the channel outlet in station x = 0.525 m, the airflow velocity is very high, especially near the bottom of the upper hot surface of the channel. These high values are the result of the deviation in the air current due to the presence of the second obstacle and also due to pressure from the middle recycling area. In the lower section of this area at the outlet of the channel, the speed values decrease due to the rear recycling area, Fig. 6 (d).

Figs. 7 (a) to (h) represent the change of axial velocity profiles in terms of the change in Reynolds number values. Eight transverse positions from different regions of the solar channel, namely x = 0.159 m, x = 0.189 m, x = 0.255 m, x = 0.285 m, x = 0.315 m, x = 0.345 m, x = 0.465 m, and x = 0.525 m, were determined by changing the number of Reynolds from 12,000 to 32000, avec an increase of 5,000. Axial velocity values increase during Reynolds number values by increasing the intensity of recycling areas in the back and front areas of the upper and lower sections of each obstacle within the channel.

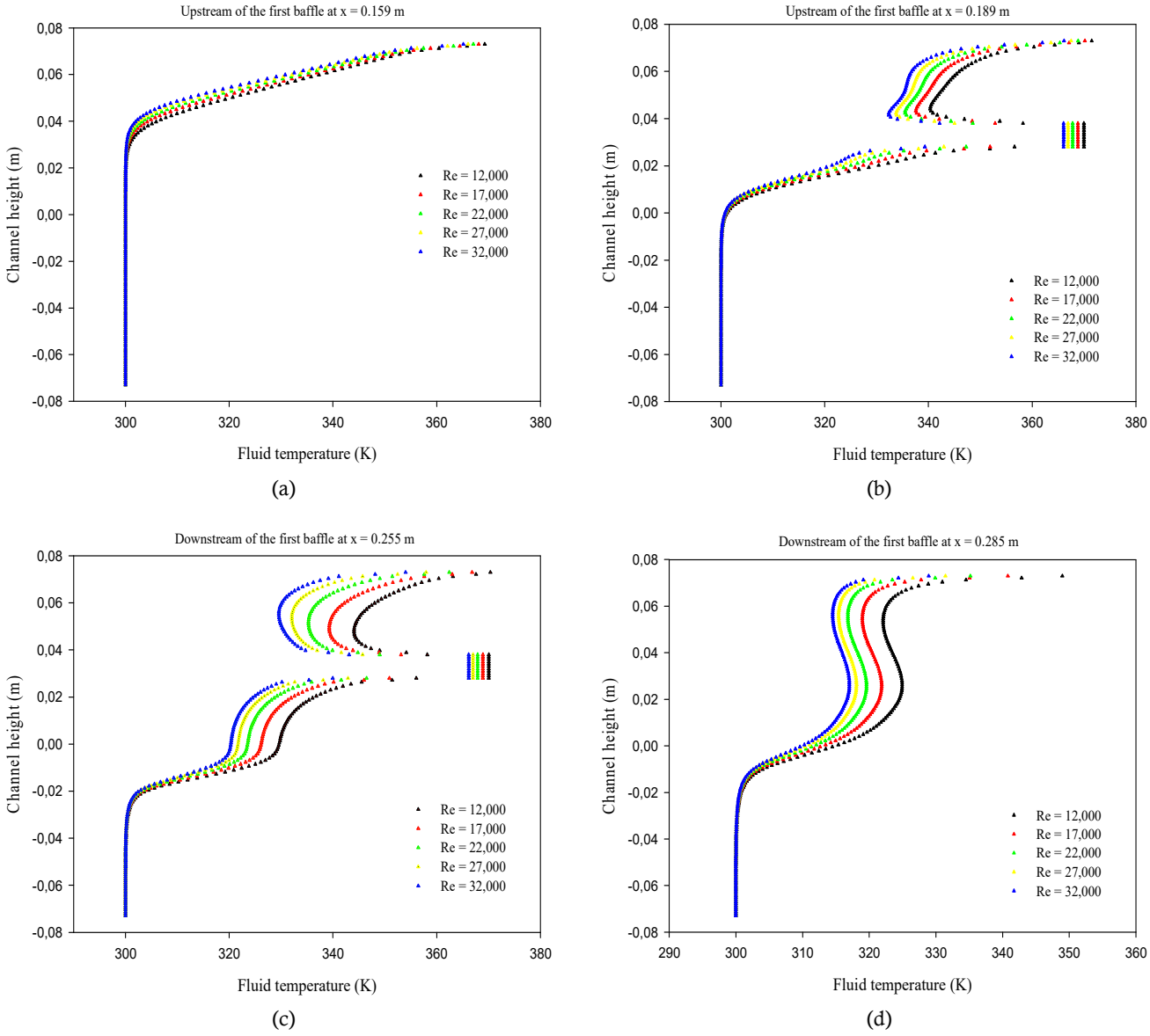

Fig. 9. Variation of fluid temperature profiles with Reynolds number at various axial stations in the channel.

Fig. 8 (a) shows the temperature profiles of the air molecules in different transverse stations of the studied solar channel. Starting with the first section of the channel, at x = 0.159 m and x = 0.189 m from the channel entrance, 0.059 m and 0.029 m before the first obstacle, 0.395 m and 0.365 m from the channel outlet, respectively, the air temperature

of the upper section of the channel rises near the hot surfaces at the recirculation zones on the left side of the first obstacle, where the current is moving in the opposite direction with low-speed rotary rings, this continuous rotation allows repeated contact of the air particles with the hot walls of the channel and the first obstacle. In the lower section of the channel, the air maintains its natural temperature due to the lack of hot areas in this area. Hot currents are close to the hot walls.

In the adjacent area of the first obstacle at the two adjacent positions x = 0.555 m and x = 0.285 m of the channel entrance, 0.027 m and 0.057 m after the first obstacle, 0.115 m and 0.085 m before the second obstacle, 0.299 m and 0.269 m of channel outlet, respectively, the temperature rises due to the presence of areas of recycling, whether weak ones on the right side of the first obstacle or strong in the area confined between the lower and upper right sides of the hot obstacle and the main stream to the left of the second obstacle. The current temperature decreases with its proximity to the thermally insulated bottom surface, Fig. 8 (b).

Near the thermally insulated obstacle attached to the bottom wall of the channel, at the level of the adjacent axial positions x = 0.315 m and x = 0.345 m of the channel entrance, the airflow temperature rises widely in this area of the channel. This rise in temperature is indicative of the presence of reverse currents in the form of powerful rotational rings, and their extension to the ends of the second obstacle in the upper section of the solar channel, Fig. 8 (c).

Next to the right side of the second obstacle at position x = 0.465 m of the channel entrance, and near its outlet in position x = 0.525 m, the air flow temperature is reduced due to high speed due to current deviation. This is due to the presence of the second obstacle and to the concentration of recycling areas in the central region of the channel and also because of the presence of the large recycling area behind the second obstacle that continues to the outlet of the channel, Fig. 8 (d).

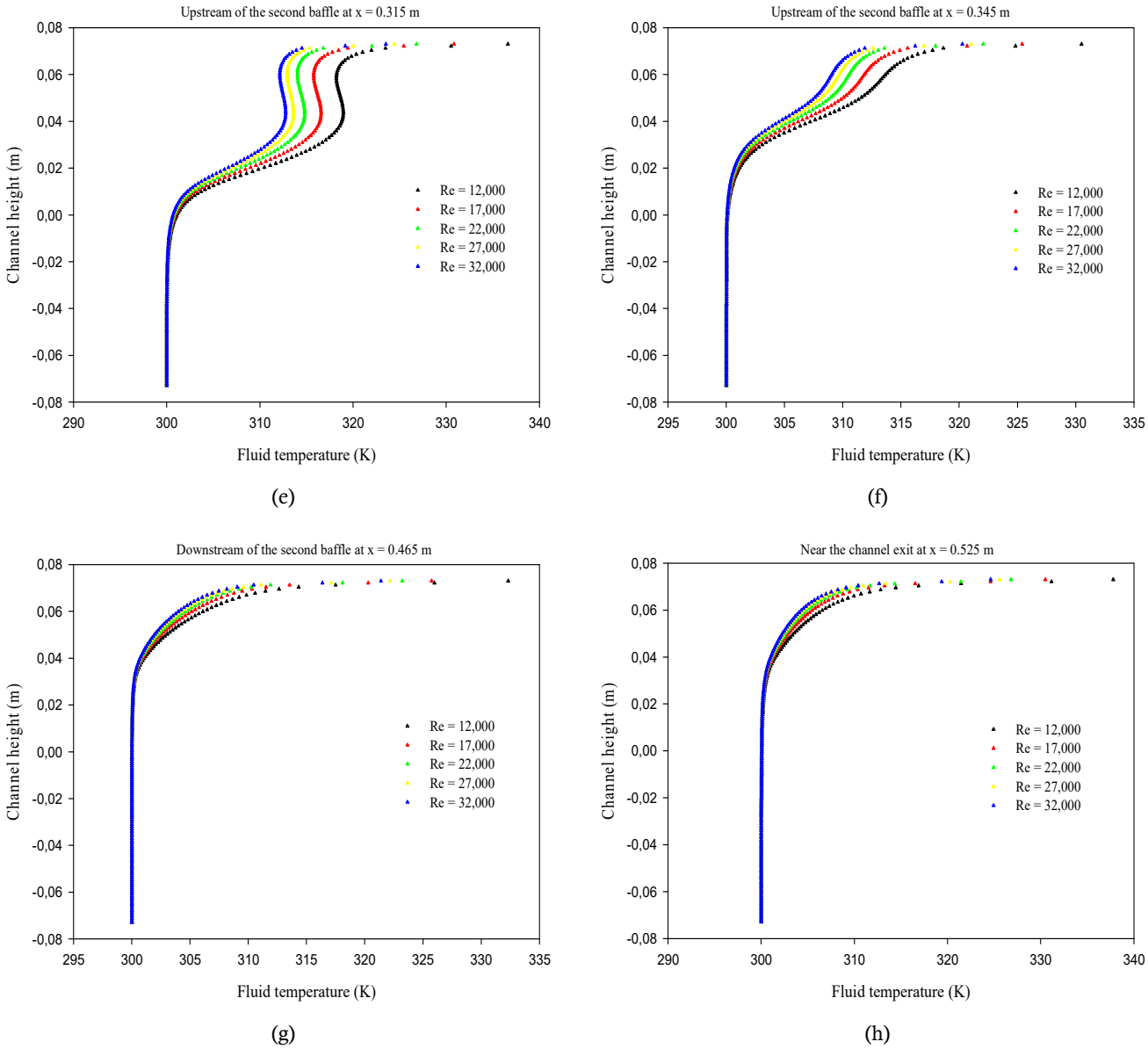

Fig. 9. Continued.

The data in Figs. 9 (a) to (h) shows the effect of Reynolds' change on the internal thermal structure of the channel. Hot areas occupy areas close to hot walls. By increasing the number of Reynolds, the flow velocity is increased, and the temperature of the air particles is reduced in the different stations studied previously, i.e., x = 0.159 m, x = 0.189 m, x = 0.255 m, x = 0.285 m, x = 0.315 m, x = 0.345 m, x = 0.465 m, and x = 0.525 m, represented in Figs. 9 (a) to (h), respectively.

The normalized local Nusselt (Nu_x) values immediately drop after the channel entrance until they are missing at the position of the first obstacle because they are located at the top of the channel allowing the current to move to the lower section, i.e., a gradual decrease in contact between the aerodynamic particles and hot areas of the upper wall of the solar channel.

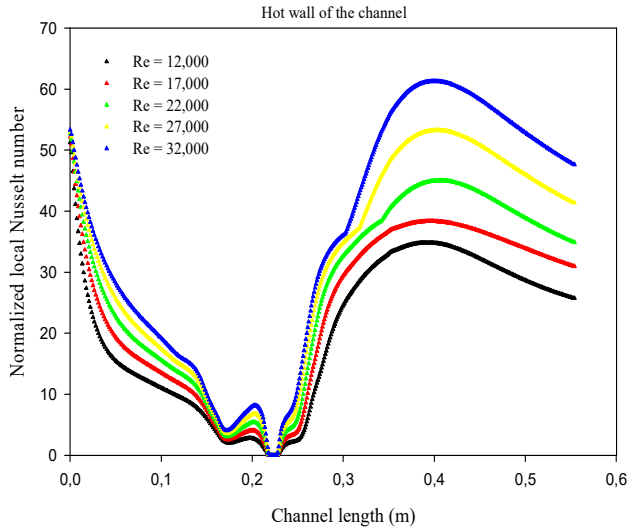

Fig. 10. Distribution of normalized local Nusselt number along the upper channel wall for various Reynolds numbers.

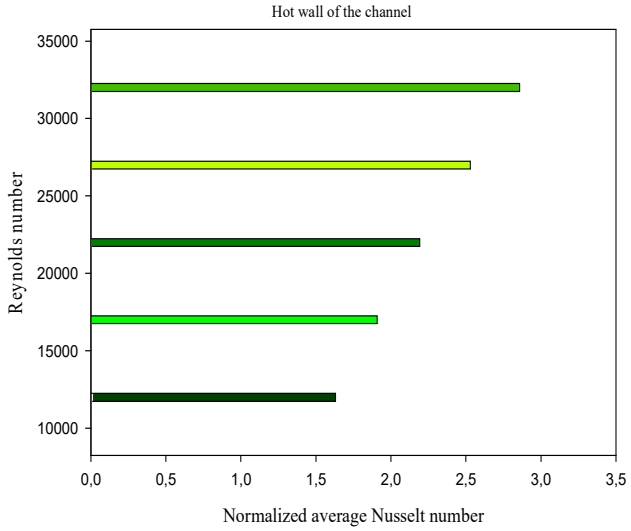

Fig. 11. Variation of normalized average Nusselt number with Reynolds number.

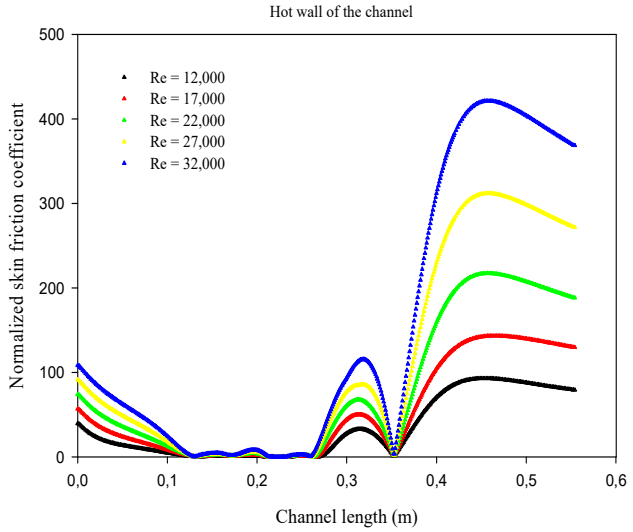

Fig. 12. Distribution of normalized skin friction coefficient along the upper channel wall for various Reynolds numbers.

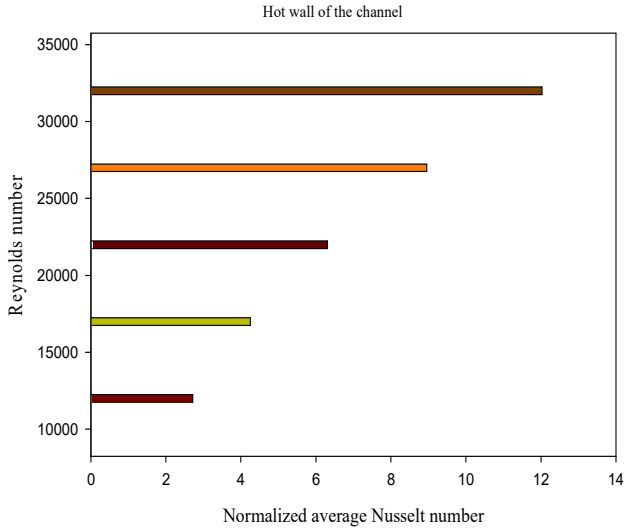

Fig. 13. Variation of normalized friction factor with Reynolds number.

The Nu_x values rise slightly near the upper right side of the first obstacle due to the presence of a small recycling area. The values of Nu_x rise over the length of the separation distance between the obstacles due to the presence of a large area and strong intensity of recycling in this aspect of the channel. These areas have a reverse movement, forming continuous rotary rings allowing for contact and friction with the hot top surface of the channel and thus good heat exchange. The Nu_x values reach their maximum value above the second obstacle due to the extreme deviation of the current from the latter towards the hot wall of the channel. The Nu_x values are gradually reduced after the second obstacle to the outlet of the channel due to the violent collision of the current with the upper wall of the channel. The path is lowered downwards next to the large recycling area and the rear of the second obstacle. To raise the Nu_x values, we increase the number of Reynolds, which increases the value of the speed at the entrance of the channel, increasing the intensity of collisions, friction and contact with the upper walls of the hot channel and thus better heat exchange, Fig. 10.

The following figure confirms these numerical results. There is a direct correlation between the values of the normalized

average Nusselt number (*Nu*) and the values of the Reynolds number (*Re*). In the case of the number of Reynolds equal 32,000, the *Nu* values increase by 42.932 %, 33.207 %, 23.303 %, and 11.497 % compared to those given by the other Reynolds values of 12,000, 17,000, 22,000 and 27,000, respectively, Fig. 11.
Skin friction (*Cf*) values increase in areas with high flow velocity. The first area is confined between the upper and lower obstacles due to the presence of a high-intensity recycling area. The second area is above the second obstacle due to the severe and strong deviation of the current because of the latter and collided with the hot top wall, Fig. 12. The *Cf* value decreases immediately after the channel entrance and after the second obstacle near its outlet. There is no friction value next to the first obstacle due to the weakness of recycling areas in this area on the left and right upper sides of the same obstacle. The *Cf* values are absent due to the lack of contact between the aerodynamic particles and the upper channel wall at the following locations: After the channel entrance between the main current and secondary stream of the recycling area on the upper side of the left side of the first obstacle. After the first obstacle between the secondary current of the recycling area on the upper side of the right side of the same obstacle, and the secondary current in the center region of the canal between the obstacles. Finally, between the strong recycling area and the main stream directed by the second obstacle toward the upper section of the channel. The *Cf* values in all positions of the upper wall of the channel increase by increasing the number of Reynolds values (see Fig. 12). These results are confirmed in Fig. 13. The mean friction (*f*) values are significant in the case of the large Reynolds number values. So the case of Re = 32,000 shows more energy loss by friction of 77.365 %, 64.606 %, 47.533 %, and 25.511 % than those of Re = 12,000, 17,000, 22,000, and 27,000, respectively.

5. Conclusion

The computational fluid dynamic data obtained for different situations selected in the '+' baffled channel and for various Reynolds number values, were represented graphically by streamlines, mean velocity fields, turbulent viscosity contours, and isotherms, as well as by axial velocity and temperature profiles, normalized local and average Nusselt numbers, and skin coefficient and factor of friction. According to analysis of numerical results on axial velocity and temperature profiles, for different sections of the channel, it was found that the temperature of the fluid is related to the velocity of flow; differently say that there is an inverse proportionality between increase in the rate of flow and reduction in the fluid temperature in each transverse section. The heat transfer rate augmented significantly and rapidly along with the second '+' obstacle and reached its maximum on its upper side because the velocity close to the top of the channel, was strongly elevated due to intense recirculation zone in the back face of this same obstacle. Concerning the pressure loss given in dimensionless form by the friction factor and for a Reynolds number range from 12,000 to 32,000, the fluid dynamic analysis showed a considerable augmentation in the normalized friction factor with the Reynolds number, introducing large recirculation zones. There exists then a direct proportionality between the skin friction increase and the elevation of the Reynolds number. Future work will involve more complex geometries and using nanofluids to assess the optimum conditions for heat transfer enhancements.

Conflict of Interest

The authors declared no potential conflicts of interest with respect to the research, authorship and publication of this article.

Funding

The authors received no financial support for the research, authorship and publication of this article.

References

[1] S.V. Patankar, C.H. Liu, and E.M. Sparrow, Fully developed flow and heat transfer in ducts having streamwise-periodic variations of cross-sectional area, *Journal of Heat Transfer*, 99(2), 1977, 180-186.
[2] M. Kelkar, and S.V. Patankar, Numerical prediction of flow and heat transfer in parallel plate with staggered fins, *Journal of Heat Transfer*, 109(1), 1987, 25-30.
[3] B.W. Webb, and S. Ramadhyani, Conjugate heat transfer in a channel with staggered ribs, *International Journal of Heat and Mass Transfer*, 28(9), 1985, 1679-1687.
[4] J.R. Lopez, N.K. Anand, and L.S. Fletcher, Heat transfer in a three-dimensional channel with baffles, *Numerical Heat Transfer*, 30(2), 1996, 189-205.
[5] S.R.N. De Zilwa, L.K. Khezzar, and J.H. Whitelaw, Flows through plane sudden-expansions, *International Journal of Numerical Method in Fluids*, 32(3), 1998, 313-329.
[6] Y.M. Hong, and S.S. Hsieh, Heat transfer and friction factor measurement in ducts with staggered and inline ribs, *Journal of Heat transfer*, 115(1), 1993, 58-65.
[7] D.D. Luo, C.W. Leung, T.L. Chan, W.O. Wong, Flow and forced-convection characteristics of turbulent flow through parallel plates with periodic transverse ribs, *Numerical Heat Transfer*, 48(1), 2005, 43-58.
[8] M. Molki, and A.R. Mostoufizadeh, Turbulent heat transfer in rectangular ducts with repeated-baffle blockages, *International Journal of Heat and Mass Transfer*, 32(8), 1989, 1491-1499.

[9] C.H. Cheng, and W.H. Huang, Laminar forced convection flows in horizontal channels with transverse fins placed in entrance regions, *International Journal of Computation and Methodology*, 16(1), 1998, 77-100.
[10] Z. Guo, and N.K. Anand, Three-dimensional heat transfer in a channel with a baffle in the entrance region, *Numerical Heat Transfer*, 31(1), 1997, 21-35.
[11] S.S. Mousavi, and K. Hooman, Heat and fluid flow in entrance region of a channel with staggered baffles, *Energy Conversion and Management*, 47(15-16), 2006, 2011-2019.
[12] M.A. Founti, and J.H. Whitelaw, Shell side flow in a model disc-and-doughnut heat exchanger, Tech. Report FS/81/37, Mech. Eng. Dept., Imperial College, London, UK., 1983.
[13] C. Berner, F. Durst, and D.M. McEligot, Flow around baffles, *Journal of Heat Transfer*, 106(4), 1984, 743-749.
[14] C. Berner, F. Durst, and D.M. McEligot, Streamwise-periodic flow around baffles. In: Proceedings of the 2nd int. conference on applications of laser anemometry to fluid mechanics, Lisbon, Portugal, 1984.
[15] J. Antoniou, and G. Bergeles, Development of the Reattached flow behind surface mounted two-dimensional prisms, *Journal of Fluids Engineering*, 110(2), 1988, 127-133.
[16] S. Acharya, S. Dutta, and T.A. Myrum, Heat transfer in turbulent flow past a surface-mounted two-dimensional rib, *Journal of Heat Transfer*, 120(3), 1998, 724-734.
[17] S.V. Möller, L.A.M. Endres, and G. Escobar, Wall pressure field in a tube bank after a baffle plate, Trans. SMiRT 15, 15 th Int. Conf. Structural Mechanics in Reactor Technology, Seoul, 7, 1999, 262-275.
[18] L.A.M. Endres, Experimental analysis of the fluctuating pressure field in tube banks subjected to turbulent cross flow, Dr. Eng. Thesis. PROMEC/UFRGS, Federal Univ. of Rio Grande do Sul, Porto Alegre-RS, Brazil (in Portuguese), 1997.
[19] L.A.M. Endres, and S.V. Möller, On the fluctuating wall pressure field in tube banks, *Nuclear Engineering and Design*, 203(1), 2001, 13-26.
[20] L.C. Demartini, Numeric and experimental analysis of pressure and velocity fields in a duct with baffle plates, M. Eng. Dissertation, PROMEC/UFRGS, Porto Alegre-RS, Brazil (in Portuguese), 2001.
[21] L.C. Demartini, H.A. Vielmo, and S.V. Möller, Numeric and experimental analysis of the turbulent flow through a channel with baffle plates, *Journal of the Brazilian Society of Mechanical Sciences and Engineering*, 26(2), 2004, 153-159.
[22] M.A. Habib, A.M. Mobarak, M.A. Sallak, E.A. Abdel Hadi, and R.I. Affify, Experimental investigation of heat transfer and flow over baffles of different heights, *Journal of Heat Transfer*, 116(2), 1994, 363-368.
[23] H. Li, and V. Kottke, Effect of baffle spacing on pressure drop and local heat transfer in shell-and-tube heat exchangers for staggered tube arrangement, *International Journal of Heat and Mass Transfer*, 41(10), 1998, 1303-1311.
[24] Y.L. Tsay, T.S. Chang, and J.C. Cheng, Heat transfer enhancement of backward-facing step flow in a channel by using baffle installed on the channel wall, *Acta Mechanica*, 174(1-2), 2005, 63-76.
[25] P. Promvonge, and C. Thianpong, thermal performance assessment of turbulent channel flows over different shaped ribs, *International Communications in Heat and Mass Transfer*, 35(10), 2008, 1327-1334.
[26] S. Sripattanapipat, and P. Promvonge, Numerical analysis of laminar heat transfer in a channel with diamond-shaped baffles, *International Communications in Heat and Mass Transfer*, 36(1), 2009, 32-38.
[27] P. Promvonge, and S. Kwankaomeng, Periodic laminar flow and heat transfer in a channel with 45° staggered V-baffles, *International Communications in Heat and Mass Transfer*, 37(7), 2010, 841-849.
[28] P. Sriromreun, C. Thianpong, and P. Promvonge, Experimental and numerical study on heat transfer enhancement in a channel with Z-shaped baffles, *International Communications in Heat and Mass Transfer*, 39(7), 2012, 945-952.
[29] Y.G. Lei, Y.L. He, P. Chu, and R. Li, Design and optimization of heat exchangers with helical baffles, *Chemical Engineering Science*, 63(17), 2008, 4386-4395.
[30] B.B. Gupta, J.A. Howell, D. Wu, and R.W. Field, A helical baffle for cross-flow micro filtration, *Journal of Membrane Science*, 102(6), 1995, 31-42.
[31] H. Benzenine, R. Saim, S. Abboudi, and O. Imine, Numerical analysis of turbulent flow and conjugate heat transfer characteristics in a channel provided with internal waved fins and baffles: effect of pitch of waved fins and baffles, in: Proceedings of ASME 2010 3rd Joint US-European fluids engineering summer meeting and 8th Int. Conf. Nanochannels, Microchannels, Minichannels FEDSM2010-ICNM2010, Montreal, Canada, 2013.
[32] Nasiruddin, and M.H. Kamran Siddiqui, Heat transfer augmentation in a heat exchanger tub using a baffle, *International Journal of Heat and Fluid Flow*, 28(2), 2007, 318-328.
[33] P. Dutta, Innovative heat transfer enhancement with inclined solid and perforated baffles, MS Thesis, South Carolina Univ., Columbia, SC., 1997.
[34] P. Dutta, and S. Dutta, Effect of baffle size, perforation and orientation on internal heat transfer enhancement, *International Journal of Heat and Mass Transfer*, 41(19), 1998, 3005-3013.
[35] P. Dutta, S. Dutta, R.E. Jones, and J.A. Khan, Heat transfer coefficient enhancement with perforated baffles, *Journal of Heat Transfer*, 120(3), 1998, 795-797.
[36] F.R. Menter, Two-equation eddy-viscosity turbulence models for engineering applications, *AIAA Journal*, 32(8), 1994, 1598-1605.
[37] S.V. Patankar, Numerical heat transfer and fluid flow, McGraw-Hill, New York, 1980.
[38] B.S. Petukhov, Heat transfer and friction in turbulent pipe flow with variable physical properties, *Advances in Heat Transfer*, 6, 1970, 503-564.

[39] F.W. Dittus, and L.M.K. Boelter, Heat transfer in automobile radiators of tubular type, University of California Publications in Engineering. Vol. 2, Berkeley, California, University of California Press, 1930.

ORCID iD

Younes Menni https://orcid.org/0000-0003-1475-3743
Ali J. Chamkha https://orcid.org/0000-0002-8335-3121
Ahmed Azzi https://orcid.org/0000-0002-0900-1996